Robustness Analysis and Reliable Flight Regime Estimation of an Integrated Resilent Control System for A Transport Aircraft

Jong-Yeob Shin*
National Institute of Aerospace, Hampton, VA 23666
Christine Belcastro †
NASA Langley Research Center, Hampton, VA 23681

Abstract

Formal robustness analysis of aircraft control upset prevention and recovery systems could play an important role in their validation and ultimate certification. As a part of the validation process, this paper describes an analysis method for determining a reliable flight regime in the flight envelope within which an integrated resilent control system can achieve the desired performance of tracking command signals and detecting additive faults in the presence of parameter uncertainty and unmodeled dynamics. To calculate a reliable flight regime, a structured singular value analysis method is applied to analyze the closed-loop system over the entire flight envelope. To use the structured singular value analysis method, a linear fractional transform (LFT) model of a transport aircraft longitudinal dynamics is developed over the flight envelope by using a preliminary LFT modeling software tool developed at the NASA Langley Research Center, which utilizes a matrix-based computational approach. The developed LFT model can capture original nonlinear dynamics over the flight envelope with the Δ block which contains key varying parameters: angle of attack and velocity, and real parameter uncertainty: aerodynamic coefficient uncertainty and moment of inertia uncertainty. Using the developed LFT model and a formal robustness analysis method, a reliable flight regime is calculated for a transport aircraft closed-loop system.

Nomenclature

Robust analysis parameters

ω	:	frequency (rad/sec)	$\mathbf{\Delta}$	:	Set of uncertainty blocks
Δ	:	uncertainty block	$\mathcal{R}$	:	Real number set
$\mathcal{C}$	:	Complex number set	$\|\|\cdot\|\|$	:	L_2 norm

*Senior Staff Scientist, Robust and Adaptive Control, AIAA Senior Member, email:shinjy@nianet.org.
†Senior Researcher, Dynamic Systems and Control Branch, AIAA Senior Member.

Aircraft parameters

α	:	angle of attack (AOA), (rad)	δ_e	:	elevator deflection, (deg)
q	:	pitch angle rate, (rad/sec)	δ_s	:	stabilizer deflection, (rad)
V	:	True airspeed, (m/sec)	T	:	thrust, (N)
θ	:	Pitch angle, (rad)	$\bar{c}$	:	mean chord length, (m)
γ	:	flight path angle, (deg)	$\bar{q}$	:	dynamic pressure, (N/m^2)
m	:	total mass, (kg)	c_7	:	inertia coefficient, $1/I_{yy}$, $(kg^{-1}m^{-2})$
S_{zeng}	:	summation of z positions of engines, (m)			

Aerodynamic coefficients

$C_{D_{Mach}}$	:	drag coefficient at fixed mach number
C_L	:	total lift coefficient
$C_{L_{basic}}$	:	lift coefficient for the rigid airplane at zero stabilizer angle
C_m	:	pitch moment coefficient
$C_{m_{basic}}$	:	pitch moment coefficient for the rigid airplane at zero stabilizer angle

1 Introduction

Aircraft loss-of-control (LOC) accidents [1–3] comprise a significant aircraft accident category across all civil transport classes, and can result from a large array of causal and contributing factors (e.g., system and component failures, control system impairment or damage, inclement weather, inappropriate pilot inputs, etc.) occurring either individually or in combination. Research [4–7] into the characterization of the aircraft LOC phenomenon as well as LOC prevention and recovery system technologies is being conducted by NASA as a part of its Aviation Safety Program (AvSP). In Ref. [8], it is shown that loss-of-control events can involve flight beyond normal operating conditions. Moreover, these conditions are not well modeled in current transport simulations. Validation of both the mathematical models and the systems technologies for LOC conditions is therefore highly nontrivial.

Certification of LOC prevention and recovery systems (including failure detection, identification, and reconfiguration as well as upset recovery subsystems) for an aircraft will require a comprehensive validation process (integrating analysis, simulation, and experimental methods) to ensure the safety and reliability of these systems over the entire flight envelope. Robustness analysis for systems with structured uncertainty could play an important role in this process. For an aircraft control system, robustness to nonlinear parameter variations over the flight envelope and at extreme flight conditions must also be considered. Ref. [9] provides an excellent treatment of applying robustness analysis methods to the clearance of flight control laws, and Ref. [5] provides a robustness analysis framework for failure detection and accommodation systems. Analytical robust control methods, such as the structured singular value method (μ-analysis method in Refs. [5, 9]), have been applied for the clearance of a flight control law in Ref. [10]. The linear fractional transformation (LFT) model of an aircraft has been constructed with a parameter uncertainty and linearized models of the aircraft at each trim condition [10]. The LFT model in Ref. [10] can capture dynamics change due to the uncertain parameters but not to flight condition variation.

One of the clearance techniques for a flight control law is polynomial-based analysis in Ref. [11] that checks the robust stability of a dynamic system by looking at the uncertain coefficients of the characteristic polynomial, which is a function of flight condition. In Ref. [11], the safety flight envelope is calculated based on the eigenvalues of the system evaluated at the given flight condition over the flight envelope using the adaptive gridding approach. In this paper, the desired performance level of a closed-loop system is represented by an induced $\mathcal{L}_2$ norm and is integrated with the robust analysis framework over the entire flight envelope. In robustness analysis of the system, the nonlinearity of the original dynamics due to flight condition variation is integrated with model uncertainty parameters. The nonlinearity and model uncertainties are represented by the Δ block of the LFT model which can capture the original nonlinear dynamics.

Formulation of the LFT model can be extremely difficult and time consuming, especially for aircraft problems involving parametric uncertainties (see Refs. [5, 9, 12–16]). In fact, the difficulty in formulating the uncertainty model in LFT form has been a key impediment to performing robustness analysis for these systems. Ref. [1] presents a numerical matrix-based modeling method and preliminary software tool for computing LFT models from a polynomial system.

In Ref. [17], an integrated fault identification and fault tolerant control system (hereafter called an IFTC system) of a transport aircraft is designed, which includes a fault tolerant control (FTC) law and fault detection and isolation (FDI) filters. In Ref. [17], the FTC law is designed as an H_∞ control law to minimize command tracking errors under actuator fault occurrence, and the FDI filter is designed based on an affine LPV model of the Boeing 747 aircraft to generate residual signals using a geometric approach [18]. The FTC law is designed based on a linearized model with given unmodeled dynamics, and is applied on the original nonlinear dynamics. Around a trim condition, the performance of the closed-loop system with the original nonlinear dynamics can be predicted but far from the trim point the performance of the closed-loop system cannot be predicted due to the nonlinearity. The conventional validation method for the closed-loop is nonlinear simulation with the pre-defined time history of command signals.

In this paper, the nonlinearity due to flight condition variation is converted into a LFT form of the system. The developed LFT model with the Δ block, which contains key parameters such as angle of attack and velocity, can capture the nonlinear dynamic variations over the flight envelope along with parameter uncertainty and unmodeled dynamics. Using the robustness analysis tool (μ-analysis), the closed-loop system can be evaluated over the flight envelope with the pre-defined performance level that is typically defined as the induced-$\mathcal{L}_2$ norm with the frequency weight function. This paper determines and presents a reliable flight regime, in which the IFTC system achieves the desired performance of command tracking and failure detection.

This paper contains the following sections. In Section 2, the LFT modeling algorithm of the matrix-based computational approach is summarized. In Section 3, the analysis problem for the IFTC system is described. In Section 4, the LFT model of the longitudinal motion of the transport aircraft in Ref.[13] is developed over the given flight envelope. In Section 5, a robustness analysis framework and the calculated reliable flight regimes are described. In Section 6, nonlinear simulation results are described, and in Section 7 the results are summarized with conclusions.

2 Numerical Parameter LFT Modeling Approach

For completeness, the matrix-based LFT modeling method presented in Refs. [1, 5] is briefly summarized. Consider a polynomial system as

$$\begin{bmatrix} \dot{x} \\ y \end{bmatrix} = \begin{bmatrix} A(\rho) & B(\rho) \\ C(\rho) & D(\rho) \end{bmatrix} \begin{bmatrix} x \\ u \end{bmatrix}, \tag{1}$$

where $\rho \in \mathcal{R}^m$ and m is the number of uncertain parameters. Assume that the matrices $A(\rho)$, $B(\rho)$, $C(\rho)$ and $D(\rho)$ are in multi-variable polynomial matrix form such as

$$\begin{bmatrix} A(\rho) & B(\rho) \\ C(\rho) & D(\rho) \end{bmatrix} = \begin{bmatrix} A_o & B_o \\ C_o & D_o \end{bmatrix} + \sum_{i=1}^{n_f} \begin{bmatrix} A_i & B_i \\ C_i & D_i \end{bmatrix} f_i(\rho), \tag{2}$$

where $f_i(\rho)$ is a multi-variable polynomial function and n_f is the total number of functions. The LFT model of the system of Eq. (1) to be solved is depicted in Fig. 1. The matrix $\Delta(\rho)$ contains the system

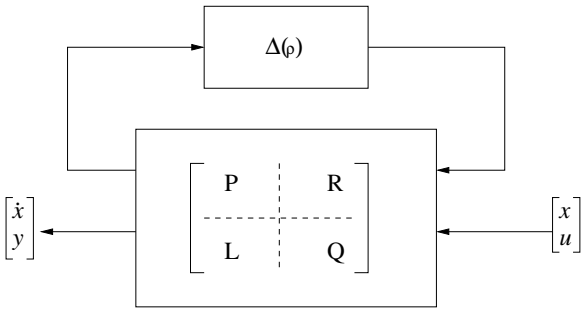

Figure 1: Block diagram of the LFT modeling problem

uncertainties, and can be represented as follows for parametric uncertainties.

$$\Delta(\rho) = \text{diag}[\delta_1 I_{n_1}, \ \delta_2 I_{n_2}, \ \cdots, \ \delta_m I_{n_m}] \tag{3}$$

$$\rho = [\delta_1, \delta_2, \cdots, \delta_m] \in \mathcal{R}^m \tag{4}$$

The LFT equation associated with Fig. 1 is given below

$$S(\rho) = L(I - \Delta(\rho)P)^{-1}\Delta(\rho)R + Q = S_\Delta(\rho) + Q, \tag{5}$$

where the matrix $S(\rho)$ is a compact representation of the system model. The matrix P, R, and L are associated with the uncertainty block $\Delta(\rho)$. The matrix Q represents the nominal system model. The matrix $S_\Delta(\rho)$ can be solved for multivariate polynomial problems by replacing the matrix inversion with a finite series expansion and a nilpotency condition,

$$S_\Delta(\rho) = L\Delta R + L[\Delta P + (\Delta P)^2 + \cdots + (\Delta P)^r]\Delta R \tag{6}$$

$$(\Delta P)^{r+1} = 0 \tag{7}$$

where r is determined by the degree of the largest nonzero term in $S_\Delta(\rho)$.

The blocks of L and R, and the main-diagonal blocks of P are solved simultaneously for each uncertain parameter δ_i using all single-parameter nth-order terms, and the off-diagonal blocks of P are each solved using the appropriate cross terms of $S_\Delta(\rho)$. The detailed procedures are described in Refs. [1, 5].

3 Analysis Problem Statement for The IFTC System

The IFTC system of the Boeing 747-100/200 aircraft presented in Ref. [17] is briefly described here to carry out the analysis problem of the system over a flight envelope. The IFTC system shown in Fig. 2 contains a fault tolerant control law, fault detection and isolation filters, actuators and sensors. In Ref. [17], the

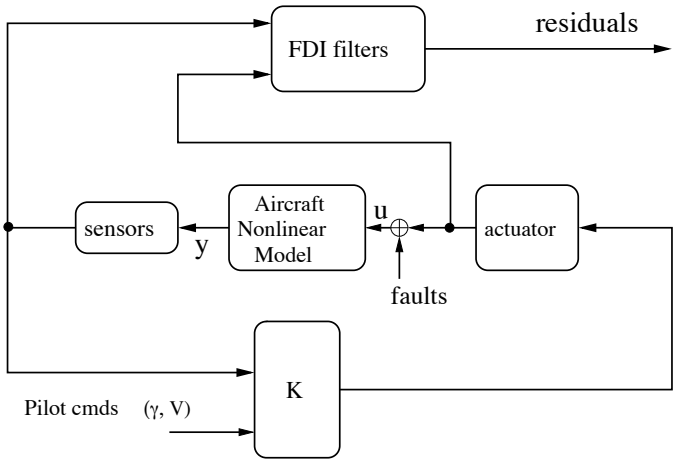

Figure 2: The simplified block diagram of the IFTC system of a transport aircraft in Ref.[13].

fault tolerant control law was designed as a passive fault tolerant control law minimizing flight-path angle and velocity command tracking errors in the presence of actuator faults. Actuator faults are modeled as additive signals on each control channel. In Ref. [17], the LPV-FDI filters were designed, based on the affine LPV model of the longitudinal motion of the Boeing 747-100/200 aircraft, as residual generators using the geometric approach [18]. Note that in this paper, the linearized FDI filters around a trim point are used for robustness analysis of the IFTC system.

In this paper, the analysis problem is considered as "in what region of the flight envelope can the designed system achieve the desired closed-loop performance level of tracking commands and detecting additive faults in the presence of parameter uncertainty and unmodeled dynamics ?". Generally, the flight region to be determined is hereafter called the reliable flight regime. The reliable flight regime is dependent on nonlinear dynamics changes over the flight envelope, the desired performance level, maximum allowable command size, additive faults, and system uncertainties.

To analyze the IFTC system over the entire flight envelope, the augmented IFTC system is constructed with performance weighing functions (W_p and W_f), a fault scale matrix (F_s), a command scale matrix (C_s) and ideal closed-loop dynamics (T_i) and is shown in Fig. 3. The performance weight function, W_p, and ideal response, T_i, can be defined to represent the desired performance, command tracking error, and the weighting function W_f can be designed based on the desired fault detection accuracy for additive faults by representing detection accuracy as the desired residual generation due to additive faults. The matrices, C_s and F_s, can represent possible maximum size of command and additive faults, respectively. Note that in the augmented closed-loop system, the nonlinear aircraft dynamics are replaced with the LFT model with the block $\Delta_{model}(\alpha,\ V)$. The block Δ_{model} is decoupled into two components: a component, $\Delta_m(\alpha, V)$, which is flight condition dependent, and an uncertainty component, Δ_{mc}, which represents real parameter uncertainty whose size is constant over the flight envelope. The block $\Delta_{model}(\alpha, V)$ is rewritten as

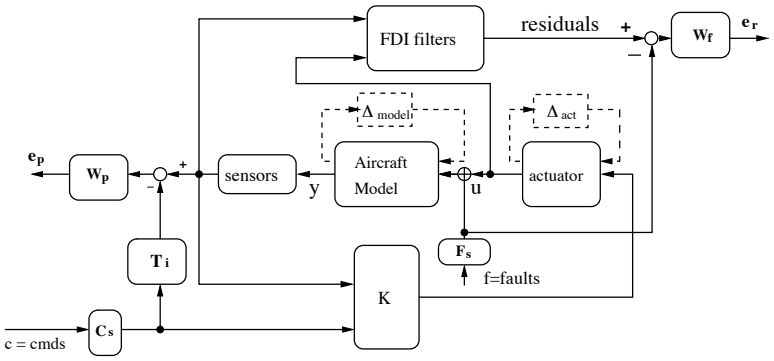

Figure 3: Augmented closed-loop interconnection block diagram of the IFTC system of a transport aircraft.

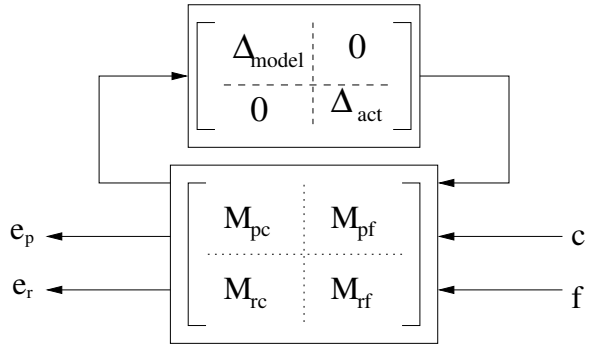

Figure 4: Generalized block diagram of the IFTC system.

$diag([\Delta_m(\alpha, V), \Delta_{mc}])$. The block Δ_{act} shown in Fig. 3 represents unmodeled actuator dynamics. The augmented IFTC system is converted into the generalized block diagram shown in Fig. 4 with the uncertain block $\Delta = diag\{\Delta_{model},\ \ \Delta_{act}\}$, which is useful for robustness analysis (μ-analysis).

For the robustness analysis of the IFTC system, robust performance in an H_∞ sense for the subsystems (M_{pc}, M_{pf}, M_{rc}, and M_{rf}) shown in Fig. 4 is interpreted as follows:

1. $\mu(M_{pc})$: Robustness to command tracking errors in control performance over the entire flight envelope in the presence of real parameter uncertainty and unmodeled dynamics.
2. $\mu(M_{rf})$: Robustness to fault detection errors in FDI filter performance over the entire flight envelope in the presence of real parameter uncertainty and unmodeled dynamics.
3. $\mu(M_{pf})$: Effect of faults on performance level at a trim condition.
4. $\mu(M_{rc})$: Effect of commands on residual signals generated by the FDI filters.

In this paper, the reliable flight envelope of acceptable command tracking error in the presence of faults and the uncertainty is defined as

$$\mathcal{E}_{pcf} \equiv \{(\alpha, V) \ \mid \ \frac{||e_p||_2}{||\ [c\ \ f]\ ||_2} \leq \beta, \ \ (\alpha, V) \in \mathcal{F}_e, \ \ \Delta_{mca} \in \mathbf{\Delta}_{mca}\} \tag{8}$$

where the set $\mathcal{F}_e$ is the entire flight envelope and the uncertainty set $\mathbf{\Delta}_{mca}$ is defined as

$$\begin{aligned} \mathbf{\Delta}_{mca} &\equiv \{diag(\Delta_{mc}, \Delta_{act})\} \\ \Delta_{mc} &= \{diag([\delta_{r1} I_1, \cdots \delta_{rn} I_n]),\ |\delta_{ri}| \leq 1,\ \delta_{ri} \in \mathcal{R}\} \\ \Delta_{act} &= \{diag([\delta_{c1}, \cdots, \delta_{cm}]),\ |\delta_{ci}| \leq 1,\ \delta_{ci} \in \mathcal{C}\} \end{aligned} \tag{9}$$

Here, δ_{ri} and δ_{ci} represent real and complex parameter uncertainties. The complex uncertainty δ_{ci} is related to unmodeled dynamics. Eq. (8) implies that the system in the reliable flight regime can achieve the desired performance level with robustness to the uncertainty described by the block Δ_{mca}.

Calculating the boundary of the set $\mathcal{E}_{pcf}$ is not easy via nonlinear simulation results since it is dependent on command time history, additive faults, and all elements of the uncertainty block Δ_{mca}. The problem is converted into calculating approximation of the set via

$$\begin{aligned} \tilde{\mathcal{E}}_{pcf} &\equiv \bigcup_i \tilde{\mathcal{E}}_{pcf,i} \\ &= \bigcup_i \{(\alpha, V) \ \mid \ \rho_{RPM}(M_{pcf}, \Delta) > 1,\ \ (\alpha, V) \in \mathcal{F}_i\} \\ &\subseteq \mathcal{E}_{pcf} \end{aligned} \tag{10}$$

where

$$\begin{aligned} \Delta &= diag([\Delta_m(\alpha, V), \Delta_{mc}, \Delta_{act}]) \\ M_{pcf} &= [M_{pc} \ \ M_{pf}] \\ \mathcal{F}_i &\equiv \{(\alpha, V) \mid \alpha_{min} \leq \alpha \leq \alpha_{max}, V_{min} \leq V \leq V_{max}\} \end{aligned} \tag{11}$$

Here, $\rho_{RPM}(M_{pcf}, \Delta)$, a robust performance margin of $\mathcal{F}_u(M_{pcf}, \Delta)$, is defined as

$$\rho_{RPM}(M_{pcf}, \Delta) = \frac{1}{max_\omega \bar{\mu}(M_{pcf})}. \tag{12}$$

with the normalized Δ.

A reliable flight regime is calculated as the following iterative process.

1. Initial $\mathcal{F}_i$ is defined as $\mathcal{F}_e$. Calculate a performance margin, ρ_{RPM}, of $\mathcal{F}_u(M_{pcf}, \Delta)$ with $(\alpha,\ V), \in \mathcal{F}_i$. Note that $\mathcal{F}_u$ denotes an upper LFT.
2. When $\rho_{RPM} \geq 1$, the subset $\mathcal{F}_i$ is in a reliable flight regime. This iteration is terminated.
3. When $\rho_{RPM} < 1$, the subset boundary $\alpha_{min}, \alpha_{max}, V_{min}$, and V_{max} are rescaled with the performance margin. This leads to a new subset, $\mathcal{F}_{i+1}$. Then go to the step one.

After this process, the set $\mathcal{F}_t$ (shown in Figure 5), one of the iteration results, is defined as

$$\mathcal{F}_t = \{(\alpha, V) \mid \alpha_{t_{min}} \leq \alpha \leq \alpha_{t_{max}},\ \ V_{t_{min}} \leq V \leq V_{t_{max}}\}. \tag{13}$$

The reliable flight region $\mathcal{E}_{pcf}$ lies between the boundary of $\mathcal{F}_t$ and $\mathcal{F}_e$ such as

$$\mathcal{F}_t \subset \mathcal{E}_{pcf} \subset \mathcal{F}_e \tag{14}$$

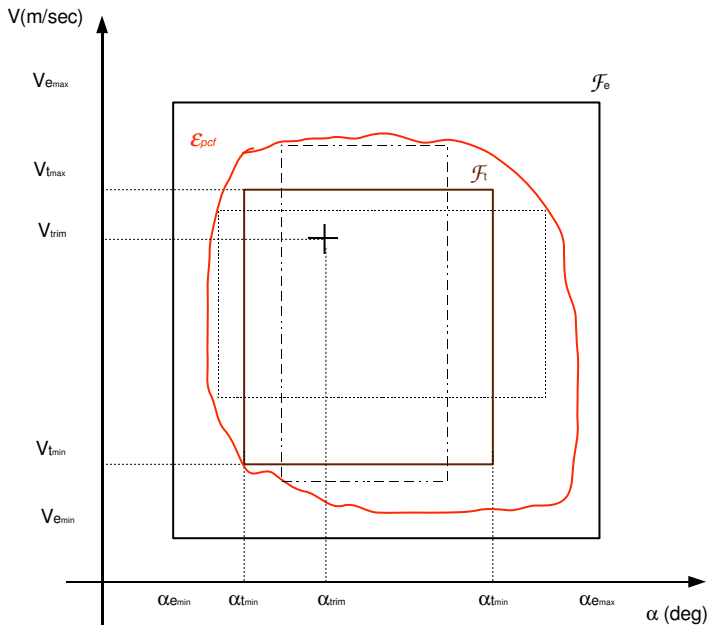

Figure 5: Illustrated plots for flight envelope and calculated subsets.

seen as the illustrated plot in Figure 5 since singular value analysis leads to conservative results of the uncertain parameter domains of $(\alpha,\ V)$. For a more accurate boundary of a calculated reliable flight regime, a reliable flight envelope subset is defined as

$$\mathcal{F}_i = \{(\alpha, V) \mid \alpha_{min} \leq \alpha \leq \alpha_{max}, V_{min} \leq V \leq V_{max}\} \tag{15}$$

where

$$\begin{aligned} \alpha_{t_{min}} \leq \alpha_{min} \leq \alpha_{trim} \qquad & \alpha_{trim} \leq \alpha_{max} \leq \alpha_{t_{max}} \\ V_{t_{min}} \leq V_{min} \leq V_{trim} \qquad & V_{trim} \leq V_{max} \leq V_{t_{max}} \end{aligned} \tag{16}$$

An optimization problem to calculate the parameters, α_{min}, α_{max}, V_{min}, and V_{max}, is formulated as

$$\min_{\alpha_{min},\alpha_{max},V_{min},V_{max}} |\rho_{RPM}(M_{pcf}, \Delta(\alpha_{min}, \alpha_{max}, V_{min}, V_{max})) - 1|. \tag{17}$$

To solve the optimization problem, the following steps are used. For example, to calculate a parameter V_{max} (unknown parameter), the other parameters are fixed as

$$\begin{aligned} \alpha_{min} &= p\alpha_{trim} + (1-p)\alpha_{t_{min}} \\ \alpha_{max} &= q\alpha_{trim} + (1-q)\alpha_{t_{max}} \end{aligned} \tag{18}$$

where p and q are any values between 0 and 1. The parameter V_{max} is calculated as

$$\min_{V_{max}} |\rho_{RPM}(M_{pcf}, \Delta(V_{max})) - 1|. \tag{19}$$

With these parameters, the set $\tilde{\mathcal{E}}_{pcf,i}$ is defined as

$$\tilde{\mathcal{E}}_{pcf,i} = \{(\alpha, V) \mid \alpha_{min} \leq \alpha \leq \alpha_{max}, \;\; V_{min} \leq V \leq V_{max}\}. \tag{20}$$

To calculate another subset $\tilde{\mathcal{E}}_{pcf,i+1}$, V_{min} is set as an unknown parameter and the other parameters are fixed. In this case, V_{max} is set as $V_{t_{max}}$. Thus, an optimization is formulated as

$$\min_{V_{min}} |\rho_{RPM}(M_{pcf}, \Delta(V_{min})) - 1|. \tag{21}$$

After this process, the sum of these subsets is shown as the dashed-dot line box in Fig. 5. The similar process is repeated for α_{min} and α_{max} at fixed V_{min} and V_{max} such as

$$\begin{aligned} V_{min} &= pV_{trim} + (1-p)V_{t_{min}} \\ V_{max} &= qV_{trim} + (1-q)V_{t_{max}} \end{aligned} \tag{22}$$

The combined set of these subsets provided with the calculated α_{min} and α_{max} is shown as the dotted line box in Fig. 5. The union of all subsets in Eq. 10 is calculated for different values of p and q in Eqs.(18) and (22), respectively.

4 LFT Modeling of the Longitudinal Motion

It is important to develop an accurate LFT model which can represent the original nonlinear dynamics of the longitudinal motion. This section presents the assumptions and procedures to reformulate the nonlinear equations of longitudinal motion into quasi-LPV polynomial form in Eq. (1). Then the LFT model is developed from the polynomial model.

4.1 High Fidelity Nonlinear Model

The full nonlinear equations of the Boeing 747 longitudinal motion are taken from Ref. [17] over the up-and-away flight regime. In this paper, the entire flight envelope $\mathcal{F}_e$ is defined as $\{(\alpha, V) \mid -2 \leq \alpha \leq 10(deg), \;\; 150 \leq V \leq 250(m/sec)\}$ at an altitude of 7000 m. The detailed nonlinear equations of motion are

$$\begin{aligned} \dot{\alpha} &= [1 - \tfrac{\bar{q}S\bar{c}}{2mV^2}(1.45 - 1.8x_{cg})\tfrac{dC_L}{dq}]q + [-\tfrac{\bar{q}S}{mV}K_\alpha \tfrac{dC_L}{d\delta_e}]\delta_e \\ &\quad + [-\tfrac{4}{mV}(\sin\alpha + 0.0436\cos\alpha)]T + \tfrac{1}{V}(\sin\alpha\sin\theta + \cos\alpha\cos\theta)g - \tfrac{\bar{q}S}{mV}C_{L_{basic}}, \end{aligned} \tag{23}$$

$$\begin{aligned} \dot{q} &= \tfrac{c_7\bar{q}S\bar{c}^2}{2V}[\tfrac{dC_m}{dq} - \tfrac{1}{\bar{c}}(1.45 - 1.8x_{c.g.})\tfrac{dC_L}{d_q}(\cos\alpha\bar{x}_{c.g.} + \sin\alpha\bar{z}_{c.g.})]q \\ &\quad + c_7\bar{q}S\bar{c}K_\alpha[\tfrac{dC_m}{d\delta_e} - \tfrac{1}{\bar{c}}\tfrac{dC_L}{d\delta_e}(\cos\alpha\bar{c}_{c.g.} + \sin\alpha\bar{z}_{c.g.})]\delta_e \\ &\quad + c_7\bar{q}S\bar{c}K_\alpha\tfrac{dC_m(h_e,M)}{d\delta_s}\delta_s + c_7S_{zeng}T + c_7\bar{q}S\bar{c}C_{m_{basic}}(\alpha, M) \\ &\quad + c_7\bar{q}S[C_{D_{Mach}}(M, C_L)(\cos\alpha\bar{z}_{c.g.} - \sin\alpha\bar{x}_{c.g.}) - C_{L_{basic}}(\alpha_w, M)(\cos\alpha\bar{x}_{c.g.} + \sin\alpha\bar{z}_{c.g.})] \end{aligned} \tag{24}$$

$$\dot{V} = \frac{4}{m}(\cos\alpha - 0.0436\sin\alpha)T + (\sin\alpha\cos\theta - \cos\alpha\sin\theta)g - \frac{\bar{q}S}{m}C_{D_{Mach}}(M, C_L) \tag{25}$$

$$\dot{\theta} = q \tag{26}$$

Note that aerodynamic coefficients and their derivatives are calculated from the look-up tables described in Ref. [19]. The detailed definitions of aerodynamic coefficients are referred to Ref. [19, 20].

4.2 Quasi-LPV Polynomial Model of the Transport Aircraft

To develop a quasi-LPV polynomial model, the aerodynamic coefficients are fit into a polynomial function form such that

$$a = [\alpha^n \;\; \alpha^{(n-1)} \;\; \cdots 1] C_a [V^m \;\; V^{(m-1)} \;\; \cdots 1]^T + \delta_a \tag{27}$$

where a is an aerodynamic coefficient, C_a is a coefficient matrix and δ_a is the fitting error which is treated here as real parameter uncertainty of the quasi-LPV model, here. The detailed polynomial fit aerodynamic coefficients are given in Ref. [20]. In this example, for simplicity, the three largest fitting errors among the aerodynamic coefficients are considered as parameter uncertainties which are not dependent on angle of attack and velocity, i.e. $|\delta_{C_{Lb}}| \leq 0.025$, $|\delta_{C_{Dm}}| \leq 0.01$, and $\delta_{C_{mq}} \in [-18.43 \;\; -17]$. With the assumption that the moment of inertia (I_{yy}) uncertainty is 5 percent of the nominal value (4527800 Kgm^2), $\delta_{I_{yy}}$ is defined. In this example, the four uncertainties are considered real parameter uncertainties.

Using the polynomial fitted aerodynamic coefficients, the longitudinal motion is rewritten as

$$\begin{bmatrix} \dot{\alpha} \\ \dot{q} \\ \dot{V} \\ \dot{\theta} \end{bmatrix} = A(\alpha, V, \delta_{mc}) \begin{bmatrix} \alpha \\ q \\ V \\ \theta \end{bmatrix} + B(\alpha, V, \delta_{mc}) \begin{bmatrix} \delta_e \\ \delta_s \\ T \end{bmatrix} + \begin{bmatrix} g/V \\ 0 \\ 0 \\ 0 \end{bmatrix}, \tag{28}$$

where $\delta_{mc} = [\delta_{C_{Lb}} \; \delta_{C_{Dm}} \; \delta_{C_{mq}} \; \delta_{I_{yy}}]^T$. The quasi-LPV model of the nonlinear polynomial model in Eq. (28) is developed using the function substitution method [19, 21–23] to convert the term g/V into quasi-LPV form. The benefit of the function substitution method is that the generated LPV model can represent the nonlinear dynamics without linear approximation (such as Jacobian linearization) over the entire possible flight region. Note that the state transformation method [21, 24, 25] can also provide an LPV representation of a nonlinear system without linear approximation. There is, however, the limitation that the LPV model should be inside equilibrium manifolds.

To apply the function substitution method, states of the model are defined as the deviation from a reference point such as

$$\tilde{\alpha} = \alpha - \alpha_t, \;\; \tilde{V} = V - V_t, \;\; \tilde{\theta} = \theta - \theta_t, \tag{29}$$

where a reference point is chosen as a trim point: $(\alpha_t, 0, V_t, \theta_t)$. Note that $\alpha_t = \theta_t$ for level flight under a trim condition. Using Eq. (29), Eq.(28) is rewritten as

$$\begin{aligned} \dot{\tilde{x}} &= A(\alpha, V, \delta_{mc})(x_t + \tilde{x}) + B(\alpha, V, \delta_{mc})(u_t + \tilde{u}) + [g/V \;\; 0 \;\; 0 \;\; 0]^T, \\ &= A(\alpha, V, \delta_{mc})\tilde{x} + B(\alpha, V, \delta_{mc})\tilde{u} + h(\alpha, V), \end{aligned} \tag{30}$$

where

$$h(\alpha, V) = A(\alpha, V)x_t + B(\alpha, V)u_t + [g/V \;\; 0 \;\; 0 \;\; 0]^T. \tag{31}$$

Note that the control $\tilde{u}$ is $[\delta_e - \delta_{e_t} \;\; \delta_s - \delta_{s_t} \;\; T - T_t]^T$ and the trim value u_t is $[\delta_{e_t}, \;\; \delta_{s_t}, \;\; T_t]^T$. Note that the stabilizer is used only as a trimming device. Thus, the control inputs are considered as elevator and thrust in this example.

After algebraic manipulations, Eq. (31) is rewritten as

$$h(\alpha, V) = \begin{bmatrix} h_\alpha \\ h_q \\ h_V \\ h_\theta \end{bmatrix} = \begin{bmatrix} 0 & h_{\alpha_V} \\ h_{q_\alpha} & h_{q_V} \\ h_{V_\alpha} & h_{V_V} \\ 0 & 0 \end{bmatrix} \begin{bmatrix} \tilde{\alpha} \\ \tilde{V} \end{bmatrix} \tag{32}$$

where the detailed function form of h_{α_V}, h_{q_α}, h_{q_V}, h_{V_α}, and h_{V_V} are omitted due to space limitations and are referred in Ref. [20]. Thus, the quasi-LPV model of the longitudinal motion of the transport aircraft in Eqs. (23)-(26) is

$$\dot{\tilde{x}} = \{A(\alpha, V, \delta_{mc}) + H(V)\}\,\tilde{x} + B(\alpha, V, \delta_{mc})\tilde{u} \tag{33}$$

where

$$H(V) = \begin{bmatrix} 0 & 0 & h_{\alpha_V} & 0 \\ h_{q_\alpha} & 0 & h_{q_V} & 0 \\ h_{V_\alpha} & 0 & h_{V_V} & 0 \\ 0 & 0 & 0 & 0 \end{bmatrix}. \tag{34}$$

The detailed component matrices are available in Ref. [20]. Note that the quasi-LPV models are functions of α, V and the selected reference point.

4.3 LFT Models of the Boeing 747-100/200 Aircraft

A LFT model is obtained and normalized from the quasi-LPV model in Eq. (33) using the numerical matrix-based LFT model tool (NT) [1] and the Robust toolbox (RT) in MATLAB, respectively. Recall that it is demonstrated in Ref. [1] that the two software tools can generate accurate LFT models which can represent the original nonlinear dynamics.

A LFT model is dependent on reference point selection since the model in Eq. (33) is dependent on a reference point which is one of the trim points. In this example, four reference points are chosen as trim points and are shown in Table 1. The four reference points are calculated to trim the aircraft dynamics at a given velocity and zero elevator deflection angle.

The developed LFT models have the block Δ_{model} such that

$$\begin{aligned} \Delta_{model} &= diag([\Delta_m(\alpha, V), \Delta_{mc}]) \\ &= diag([\delta_v I_{6\times 6},\ \delta_\alpha,\ \delta_{C_{Lb}}\ \delta_{C_{Dm}}\ \delta_{C_{mq}}\ \delta_{I_{yy}}]) \end{aligned} \tag{35}$$

where $V_{min} \le \delta_V \le V_{max}$ and $\alpha_{min} \le \delta_\alpha \le \alpha_{max}$.

5 Reliable Flight Regime Analysis Results

To calculate a reliable flight regime of the IFTC system of the aircraft, the desired performance levels are required, which are described by the weighting functions in Fig. 3. The command tracking performance

Reference points	α (deg)	V (m/sec)	δ_e (deg)	δ_s (deg)	T (N)
point 1 (P1)	4.1	180	0	-0.3	4.6 $\times 10^4$
point 2 (P2)	2.6	200	0	0.1	4.1 $\times 10^4$
point 3 (P3)	1.7	215	0	0.4	4.1 $\times 10^4$
point 4 (P4)	0.9	230	0	0.7	4.3 $\times 10^4$

Table 1: Four reference points

weighting function W_p is defined as

$$W_p = diag(\frac{40(s/100+1)}{s/0.005+1}, \frac{100(s/100+1)}{s/0.005+1}) \tag{36}$$

to allow the flight path angle and the velocity to track their commands in the 2.5% and 1 % error ranges over the low frequency region, respectively. The block T_i in Fig. 3 describes the ideal command tracking responses of γ and V, which is selected as

$$T_i = diag(\frac{0.35^2}{s^2+0.7s+0.35^2}, \frac{0.15^2}{s^2+0.3s+0.15^2}), \tag{37}$$

the second order transfer functions for the ideal closed-loop responses of γ and V. The desired performance level is defined as the error between the ideal response and the closed-loop measurement described as an induced $\mathcal{L}_2$ norm value. Recall that the matrix C_s represents allowable maximum size of command signals (γ_{cmd} and V_{cmd}). Here, three cases are considered as follows:

$$C_{s1} = diag(1\ deg,\ \ 1\ m/sec) \tag{38}$$
$$C_{s2} = diag(5\ deg,\ \ 5\ m/sec) \tag{39}$$
$$C_{s3} = diag(10\ deg,\ \ 10\ m/sec). \tag{40}$$

The fault scale matrix F_s in Fig. 3 is set as $diag(10,\ \ 10000)$ to represent 10 deg and 10000 N additive faults in the elevator and the throttle channels, respectively. The fault detection weighting function W_f is chosen as

$$W_f = diag(\frac{0.35(s/1000+1)^2}{(s/0.5+1)^2}, \frac{0.002(s/1000+1)^2}{(s/0.1+1)^2}) \tag{41}$$

to represent about 3 deg and 500 N detection errors for 10 deg elevator fault and 10000 N throttle fault, over the low frequency range. The actuator models [17] are $\frac{37}{s+37}$ for the elevator actuator and $\frac{0.5}{s+0.5}$ for the throttle actuator. Here, the unmodeled actuator dynamics are defined as $diag(\frac{0.1(s/10+1)}{s/500+1}, \frac{0.1(s/10+1)}{s/500+1})$ to represent 10% unmodeled dynamics over the low frequency range ($< 10\ r/s$) and 500% over the high frequency range ($> 500\ r/s$). The uncertainty associated with the unmodeled dynamics is defined as a complex number, $\Delta_{act} = diag(\delta_1, \delta_2), \delta_{1,2} \in \mathcal{C}$. The sensor model is approximated as an ideal sensor for consistency with Ref. [17].

The μ upper bound of each subsystem with the block $\Delta = diag([\Delta_{model}, \Delta_{act}])$ is calculated using the Robust Toolbox over the entire flight envelope and shown in Table 2. It is noticed from Table 2 that the μ upper bounds for subsystems are dependent on reference point selection. The nominal dynamics of the LFT

reference points	$\bar{\mu}(M_{pc})$	$\bar{\mu}(M_{pf})$	$\bar{\mu}(M_{pcf})$	$\bar{\mu}(M_{rc})$	$\bar{\mu}(M_{rf})$	$\bar{\mu}(M_{rcf})$
point 1 (P1)	1.21	1.17	1.23	3.77	1.15	3.77
point 2 (P2)	1.11	1.09	1.12	3.64	1.10	3.64
point 3 (P3)	1.11	1.10	1.11	3.40	1.11	3.40
point 4 (P4)	1.04	1.04	1.04	3.12	1.05	3.12

Table 2: μ upper bounds ($\bar{\mu}$) for each subsystem at each reference point with the command scale C_{s2}

	$\bar{\mu}(M_{pcf})$			$\bar{\mu}(M_{rcf})$		
reference points	C_{s1}	C_{s2}	C_{s3}	C_{s1}	C_{s2}	C_{s3}
point 1 (P1)	1.17	1.23	1.59	1.76	3.77	5.28
point 2 (P2)	1.09	1.12	1.50	1.76	3.64	5.09
point 3 (P3)	1.10	1.11	1.41	1.62	3.40	4.73
point 4 (P4)	1.04	1.04	1.32	1.55	3.12	4.31

Table 3: μ upper bounds ($\bar{\mu}$) for each subsystem at each reference point with the different command matrices.

model are defined by the selection of the reference point and the block Δ_{model} of the LFT model captures the nonlinear dynamics from the nominal dynamics. Thus, the calculated μ upper bound of subsystems can vary with reference points.

It is observed from Table 2 that the μ upper bounds of M_{pcf} are less than or equal to 1.23 for all cases. This means that the closed-loop system has robust performance in tracking commands with small degradation in the presence of faults, real parameter uncertainties, and unmodeled actuator dynamics. $\bar{\mu}(M_{pc})$ in Table 2 represents robust command tracking in the presence of real parameter uncertainties and unmodeled actuator dynamics over the entire flight envelope. $\bar{\mu}(M_{pf})$ in Table 2 represents the fault effect on command tracking, which is shown as small values in Table 2. This means the closed-loop system is a fault tolerant system with robustness to the real parameter uncertainties and actuator unmodeled dynamics over the entire flight envelope with small performance degradation.

It is observed from Table 2 that the μ upper bounds of M_{rcf} are larger than or equal to 3.12 for all cases. This implies that the FDI filters have large performance degradation on detecting additive faults. The large $\bar{\mu}(M_{rcf})$ in Table 2 are caused by the large $\bar{\mu}(M_{rc})$ which represents the coupling effect between command signals and residual signal generation. The small $\bar{\mu}(M_{rf})$ imply that the FDI filter can detect the additive fault within the pre-defined accuracy range (defined by W_f) in a steady state condition (zero command signals). To show the command signal size effect on robustness of subsystems, the μ upper bounds of the subsystems are calculated with different command cases: C_{s1}, C_{s2}, and C_{s3} defined in Eqs. (38)-(40), and are shown in Table 3. It is observed from Table 3 that the larger allowable command signals lead to more performance degradation and less performance robustness. Since the command signals affect residual signals of the FDI filters, the large variation on $\bar{\mu}(M_{rcf})$ is observed from Table 3 at a reference point. Now, reliable flight regimes for the fault tolerant control subsystem, M_{pcf}, are calculated using the method described in

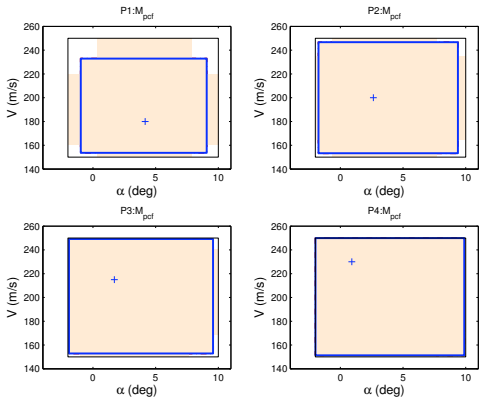

Figure 6: The reliable flight regimes for M_{pcf} due to different reference points (symbol "+") with the allowable commanding signal size C_{s2}.

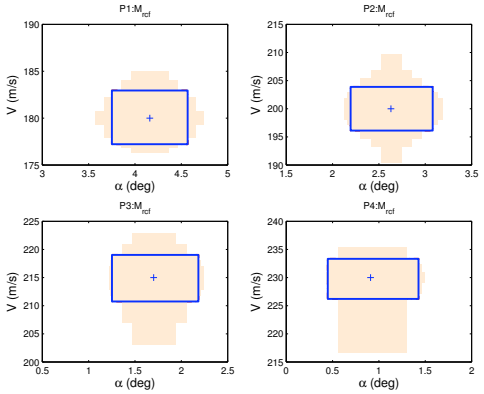

Figure 7: The reliable flight regimes for M_{rcf} at the different reference points with the allowable commanding signal size C_{s2}.

Section 3 and shown in Fig. 6. $P1$, $P2$, $P3$, and $P4$ in Fig. 6 represent reference points given in Table 1 and are shown as the "+" symbol. The solid rectangular line represents a reliable flight envelope calculated by the first iterative method. Using the method described in Section 3, the shaded regions are calculated as the subsets of the reliable flight envelope in this example. Reliable flight regimes for the FDI subsystem M_{rcf} are calculated and are shown in Fig. 7. This reliable flight regime is much smaller than that for the subsystem M_{pcf} due to the large command effect on residual signal generation. Based on Figs. 6 and 7, it can be predicted that when γ_{cmd} and V_{cmd} are set as large signals as in the C_{s3} case, the trajectory of V and α could be outside of the calculated reliable flight regime of M_{rcf} and inside of the reliable flight regime of M_{pcf}. The tracking error is expected to be small enough to achieve the pre-defined performance level (defined by W_p). It is, however, expected that the residual signals is varied due to variation in the command signals. This expected behavior will be validated via nonlinear simulation in the next section.

6 Simulation Results

The IFTC system is simulated with different magnitudes of flight path angle and velocity commands in the presence of elevator and thrust faults. For all simulations, the elevator fault is set as a step signal with 10 deg magnitude at 35 sec and the thrust fault is set as a step signal with 1000 N magnitude at 75 sec. The closed-loop system is simulated with zero command signals ($\gamma_{cmd} = 0$, $V_{cmd} = 0$) and the above faults at each of the reference points. Simulation results are shown in Fig. 8. It is observed from Fig. 8 that the thrust residual signals generated by the FDI filters are within 500 N error accuracy range for all reference points. It is also observed that there is a small coupling effect of the elevator faults at 35 sec. The elevator residual signals are also followed with the fault signals within a 3 deg error range for all reference points. The simulation results are matched with the robustness analysis results (Table 2) that $\bar{\mu}(M_{rf})$ is less than 1.15 for all reference points. Note that the real parameter uncertainty is set as the worst-case uncertainty values from the robustness analysis results, i.e., $\Delta_{mc} = diag([-0.2, 0.4, -0.3, 1])$, for all simulations. The

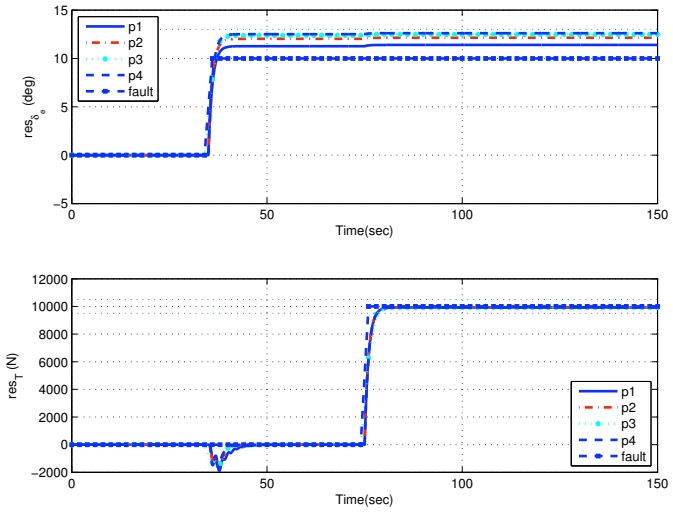

Figure 8: Residual signals at different reference points.

closed-loop system is simulated with the command signals in the presence of faults at reference point 1. For all simulations, the flight path angle command is an 85 sec duration pulse beginning at 15 sec with 1 deg (C_{s1}), 5 deg (C_{s2}), and 10 deg (C_{s3}) magnitudes. The velocity command is a step at 75 sec with 1 m/sec (C_{s1}), 5 m/sec (C_{s2}), and 10 m/sec (C_{s3}) step sizes. The V and γ time responses to the command signals are shown in Fig. 9. In the top plots, the dashed lines represent command signals for C_{s1}, C_{s2} and C_{s3} cases, respectively. It is observed from the top plots that the closed-loop system can track the command signals within the desired performance level in the presence of the additive faults. Small oscillatory time responses of the γ signals are observed at 35 sec due to the additive elevator faults. The bottom plots in Fig. 9 show the residual signals generated by the FDI filters for each case. The dashed line presents the additive faults. The elevator residual signals can detect the fault signal within 3 deg accuracy. However, the thrust residual signals cannot follow the thrust fault signals. It is observed from Fig. 9 that the thrust residual signals have been affected by γ command signals. The simulation results are matched with the robustness analysis results of Table 3.

The trajectories of V and α for each time response of the closed-loop system are shown in Fig. 10 with the

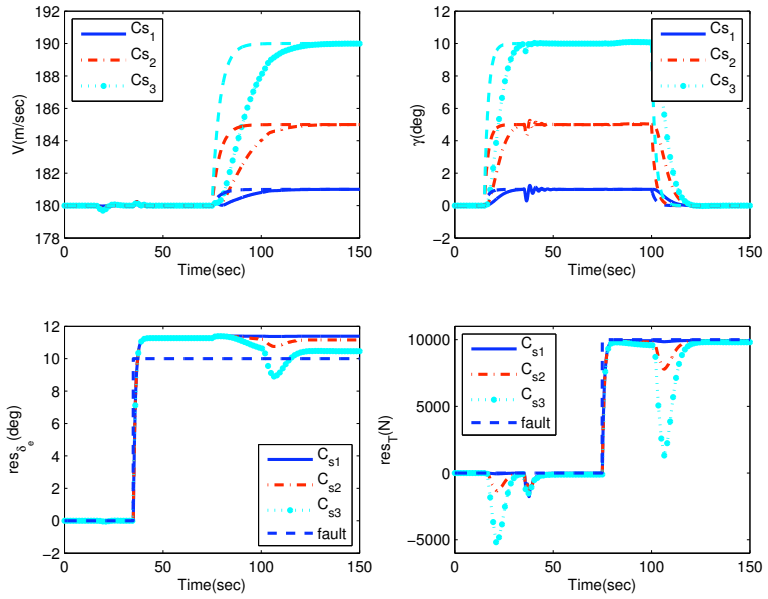

Figure 9: Simulation results with different magnitude command signals.

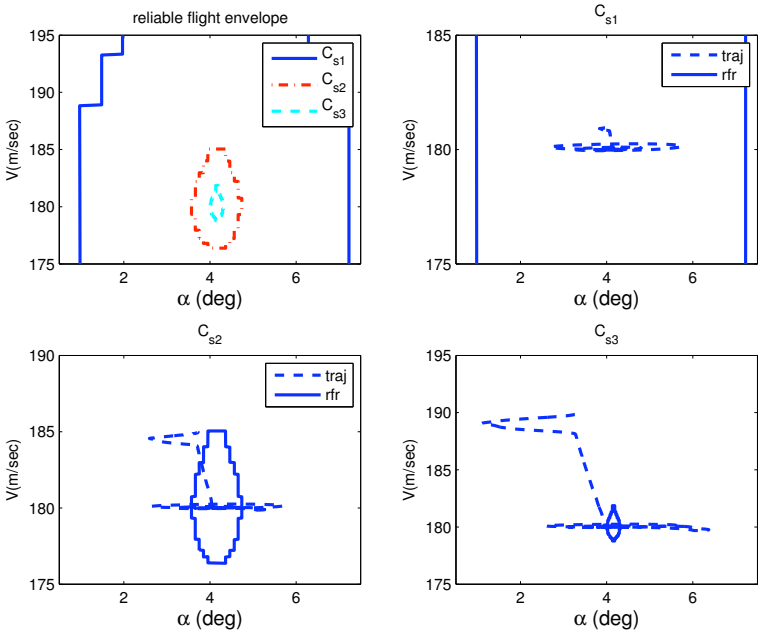

Figure 10: Trajectories and reliable flight regimes for command signals.

reliable flight regime for M_{rcf} calculated in Section 5. The left top plot in Fig. 10 shows reliable flight regimes for command cases C_{s1}, C_{s2}, and C_{s3} at the reference point, $P1$. The largest command case C_{s3}, leads to the smallest reliable flight regime due to the command effect on the residual signals. The right top plots in Fig. 10 shows that the trajectory is inside the reliable flight regime for C_{s1}. It implies that the residual signals can detect the faults within the pre-defined accuracy (W_f). It is matched with the simulation results on the bottom plot of Fig. 9. The left bottom plot of Fig. 10 shows that the trajectory is not inside the calculated reliable flight regime for C_{s2}. The right bottom plot shows that most of the trajectory is outside the calculated reliable flight regime for C_{s3}. These lower plots imply that the FDI filters cannot generate residual signals within the pre-defined accuracy range for these command cases (C_{s2} and C_{s3}). These results are matched with the time responses in Fig. 9 and the robust analysis results in Table 3.

7 Conclusion

In this paper, using the robust analysis tool, we calculate a reliable flight regime within the flight envelope of the IFTC system in which the desired performance level can be achieved in the presence of parameter uncertainty and unmodeled dynamics. To use the robust analysis tool, a LFT model of the longitudinal motion of a transport aircraft is generated based on polynomial quasi-LPV models which are developed for several reference points. Using the well-developed μ analysis method, the robustness of command tracking error, effect of command on fault detection errors, effect of fault on command tracking error, and fault detection error are calculated as μ upper bounds over the flight envelope in the presence of real parameter uncertainties and unmodeled dynamics. Using the presented analysis framework, the IFTC system of the transport aircraft is analyzed. The robust analysis results and the reliable flight regime analysis results are verified with nonlinear simulations of the closed-loop system. This analysis method could be extended to also consider robustness under noise or external disturbances (which are notoriously challenging for failure detection). This analysis approach could be used for pre-flight test check-out, as well as part of a fully-developed validation and verification process. Future research will consider performance under highly nonlinear flight regimes as a part of the analysis.

Acknowledgments

This research was supported by National Aeronautics and Space Administration under NASA Contract No. NAS1-02117. The first author thanks the technical monitor Dr. Gregory at the NASA Langley Research Center. Authors specially thank Dr. Andres Marcos and the research group of Dr. Balas at the University of Minnesota for the nonlinear simulation of the IFTC system.

References

[1] Belcastro, C., Khong, T., Shin, J-Y, Balas, G., Kwatny, H., and Chang, B., "Uncertainty Modeling for Robustness Analysis of Control Upset Prevention and Recovery Systems," in *AIAA Guidance, Navigation and Control Conference*, AIAA 2005-6427, 2005.

[2] Ranter, H., Airliner Accident Statistics 2006, in *Aviation Safety Network*, 2007.

[3] National Transportation Safety Board, Aviation Accidents from the past 10 years, in *National Transportation Safety Board*, 2007.

[4] Shin, J-Y., N.E. Eva, and Belcastro, C., "Adaptive Linear Parameter Varying Control Synthesis for Actuator Failure," *Journal of Guidance, Control, and Dynamics*, Vol. 27, Sept.-Oct. 2004, pp. 787–794.

[5] Belcastro, C. and Chang, B-C., "Uncertainty Modeling for Robustness Analysis of Failure Detection and Accommodation Systems," in *IEEE American Control Conference*, Vol. 6, American Control Conference, 2002, pp. 4776–4782.

[6] Jordan, T., Langford, W., and Hill, J., "Airborne Subscale Transport Aircrat Research Testbed- Aircraft Model Development," in *AIAA Guidance, Navigation and Control Conference*, AIAA-2005-6432, 2005.

[7] Bailey, R., Hostetler, R., Barnes K., Belcastro, Celeste, and Belcastro, Christine, "Experimental Validation: Subscale Aircraft Ground Facilities and Integrated Test Capability," in *AIAA Guidance, Navigation and Control Conference*, AIAA-2005-6433, 2005.

[8] Foster, J., Cunningham, K., Fremaux, C., Shah, G., Stewart, E., and Wilborn, J., "Dynamic Modeling and Simulation of Large Transport Airplanes in Upset Conditions," in *AIAA Guidance, Navigation and Control Conference*, AIAA-2005-5933, 2005.

[9] Christopher, F., Andras, V., Bennani, S., and Selier, M., eds., *Advanced Techniques for the Clearance of Flight Control Laws.* Spinger, 2002.

[10] Bates, D.G., Kureemun, R., and Mannchen, T., "Improved Clearance of a Flight Control Law Using μ-Analysis Techniques," *Journal of Guidance, Control, And Dynamics*, Vol. 26, Nov.-Dec. 2003, pp. 869–884.

[11] Corraro, F. and Virgilio, M., "A Polynomial Based Clearance Method," in *AIAA Guidance, Navigation, and Control Conference and Exhibit*, Aug. 2003. AIAA 2003-5479.

[12] Morton, B. and McAfoos, R., "A Mu-test for Robustness Analysis of Real-parameter Variation Problem," in *Proceedings of the American Control Conference*, Vol. 1, 1985, pp. 135–138.

[13] Morton, B., "New Application of mu to real-parameter Variations Problems," in *IEEE Conference on Decision and Control*, (Fort Lauderdale, FL), 1985.

[14] Belcastro, C., "On the Numerical Formulation of Parametric Linear Fractional Transformation (LFT) Uncertainty Models for Multivariated Matrix Polynomial Problems," NASA, , November 1998. NASA TM-1998-206939.

[15] Belcastro, C., Lim, K., and Morelli, E., "Computer-Aided Uncertainty Modeling of Nonlinear Parameter-Dependent Systems, Part I: Theoretical Overview," in *Proceeding of the Computer Aided Control System Design Conference*, August 1999.

[16] Belcastro, C., Lim, K., and Morelli, E., "Computer-Aided Uncertainty Modeling of Nonlinear Parameter-Dependent Systems, Part II:F-16 Example," in *Proceeding of the Computer Aided Control System Design Conference*, August 1999.

[17] Szaszi, I., Marcos, A., Balas, G., and Bokor, J., "Linear Parameter-Varying Detection Filter Design for a Boeing 747-100/200 Aircraft," *Journal of Guidance, Control, and Dynamics*, Vol. 28, No. 3, 2005, pp. 461–470.

[18] Balas, G., Bokor, J., and Szabo, Z., "Failure Detection for LPV Systems-A Geometric Approach," in *Proceedings of the American Control Conference*, Vol. 6, 2002, pp. 4421–4426.

[19] Marcos, A. and Balas, G., "Linear Parameter Varying Modeling of the Boeing 747-100/200 Longitudinal Motion," in *AIAA Guidance, Navigation and Control Conference*, AIAA-01-4347, American Institute of Aeronautics and Astronautics, (Montreal, Canada), Aug. 2001.

[20] Shin, J-Y., Belcastro, C., and Khong, T., "Closed-Loop Evaluation of An Integrated Failure Identification And Fault Tolerant Control System for A Transport Aircraft," in *AIAA Guidance, Navigation and Control Conference*, AIAA-2006-6310, (Keystone, CO), 2006.

[21] Shin, J-Y., *Worst-case Analysis and Linear Parameter Varying Control of Aerospace System*. PhD thesis, Department of Aerospace Engineering and Mechanics, University of Minnesota, 2000.

[22] Shin, J-Y., Balas, G.J., and Kaya, M.A., "Blending Methodology of Linear Parmeter Varying Control Synthesis of F-16 Aircraft System," *Journal of Guidance, Control, and Dynamics*, Vol. 25, No. 6, 2002, pp. 1040–1048.

[23] Shin, J-Y. and Belcastro, C., "Quasi-Linear Parameter Varying Representation over Non-trim Region," in *AIAA Guidance, Navigation and Control Conference*, AIAA-2004-5423, (Providence, Rhode Island), 2004.

[24] Papageorgiou, G. and Glover, K., "Design, Analysis and Flight Testing of a Robust Gain Scheduled Controller for the VAAC Harrier," Department of Engineering, University of Cambridge, , 2000. Technical Report CUED/F-INFENG/TR. 368.

[25] Shamma, J. and Cloutier, J., "Gain-Scheduled Missile Autopilot Design Using Linear Parameter Varying Transformations," *Journal of Guidance, Control, and Dynamics*, Vol. 16, No. 2, 1993, pp. 256–261.